ChemComm

Accepted Manuscript

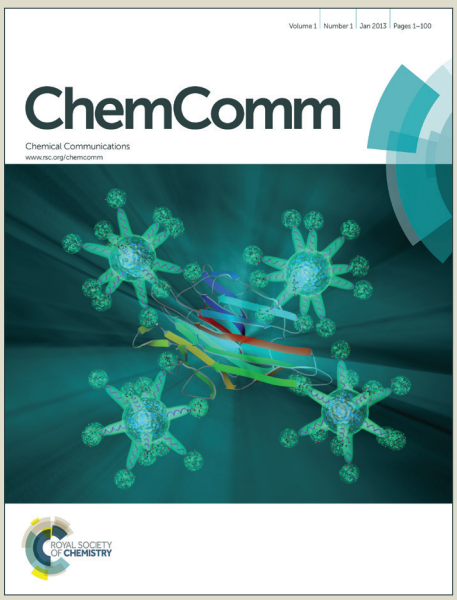

ROYAL SOCIETY OF CHEMISTRY

www.rsc.org/chemcomm

Journal Name

RSCPublishing

COMMUNICATION

Continuous synthesis of graphene sheets by spray pyrolysis and their uses as catalysts for fuel cells†

Cite this: DOI: 10.1039/xoxxoooooox

Biao Zou, Xiao Xia Wang, Xin Xin Huang, Jian Nong Wang*

Graphene sheets (GNS) were synthesized continuously by spray pyrolysis of iron carbonyl and pyridine. The Pt catalyst supported on GNS exhibited an excellent durability for oxygen reduction reaction (ORR). The GNS, when used as a metal-free catalyst for ORR, showed a performance even better than the commercial Pt/C catalyst.

Graphene, a single-atom-thick sheet with a two dimensional hexagonal structure, has attracted tremendous attentions, due to its special physical and chemical properties, such as the outstanding electronic transport capability, thermal conductivity, mechanical strength and specific surface area.[1-4] To date, many methods have been developed to prepare graphene. Mechanical exfoliation has been proved to be a good approach to prepare graphene with high quality.[5] Moreover, monolayer graphene could be exfoliated from graphite in some solvents by ultrasonication.[6] But the yield of graphene by this physical exfoliation was extremely low and also affected by the solvent used. To address this issue, chemical methods have been proposed. A typical example is the reduction of graphene oxide (GO), which can be used to achieve mass production of graphene sheets (GNS).[7] Unfortunately, the prepared GNS had a large amount of structural defects, resulting in a poor graphitic structure and thus poor electrical and chemical properties.[8,9] Chemical vapor deposition (CVD) has been used to prepare large-area GNS. This is based on the deposition on an immovable substrate, such as Ni, Ru, Ir, Cu, Pt, and SiC.[10-15] It was found to be difficult to control the thickness of GNS and remove the substrate, and the size was limited by the size of the substrate used. Apparently, the preparation of GNS with a well-developed graphitic structure, particularly in a continuous mode which is essential for large scale production, is still lacking and thus needs investigations.

In this communication, we report a novel strategy to continuously prepare high-quality GNS with a well-developed graphitic structure. This was achieved by spray pyrolysis of a mixture of iron pentacarbonyl ($Fe(CO)_5$) and pyridine (C_5H_5N). Iron nanoparticles from $Fe(CO)_5$ served as substrates for the deposition of carbon atoms from C_5H_5N. Carbonyl and pyridine were mixed at different volume ratios and pyrolysized at different temperatures. Typical experiments are listed as G1 (100:1, 900 °C), G2 (50:1, 900 °C), G3 (25:1, 900 °C), and G4 (100:1, 1000 °C).

Nano-X Research Center, School of Mechanical and Power Engineering, East China University of Science and Technology, 130 Meilong Road, Shanghai 200237, P. R. China.
* E-mail for Jian Nong Wang: jnwang@ecust.edu.cn
†Electronic Supplementary Information (ESI) available: Experimental procedures and characterization. See DOI: 10.1039/c000000x/

The reaction solutions were supplied from the top of a quartz reactor, and samples were continuously collected at the bottom. After the removal of Fe substrates, GNS with several graphitic layers were obtained. (See ESI† for experimental details and Fig. S1.)

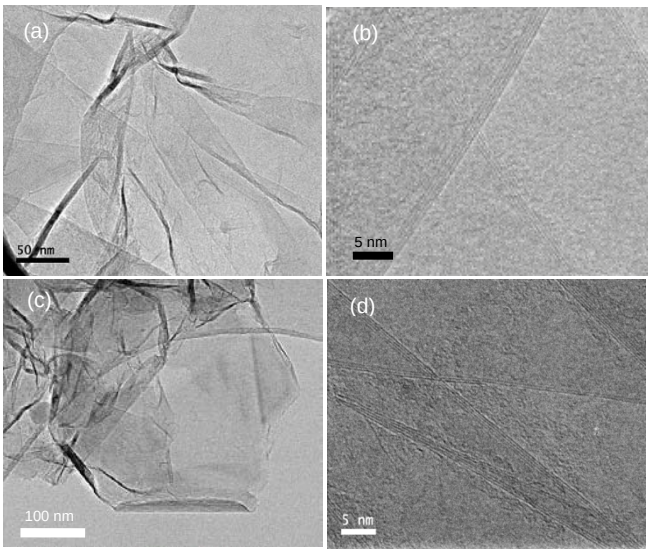

Fig. 1. TEM images of G1 (a, b) and G2 (c, d).

Transmission electron microscopy (TEM, JEM-2100) was employed to characterize the morphologies of the samples. Samples G1 (Fig. 1a,b) and G2 (Fig. 1c,d) exhibited a thin sheet structure. The sheets had a thickness of about 1.4 nm, corresponding to several graphitic layers. Except for such GNS, no iron particles were observed. As to the sample of G2, atomic force microscope (AFM, Veeco/DI) characterization further demonstrated that the sample possessed a flake-like structure and the thickness of the GNS (Fig. S2, ESI†) was ~2.0 nm. This result also suggests that the GNS consisted of several graphitic layers. Raman spectroscopy was used to investigate the graphitic structure of GNS. The Raman spectrum for G2 (Fig. S3, ESI†) shows three strong peaks at 1350, 1578 and 2703 cm^{-1}, which are designated as D, G, and 2D peaks, respectively. The D peak is related to the amount of defects, while the G peak to the amount of sp^2 hybrid carbon atoms. Therefore, the ratio between the intensities of G and D peaks is often used to estimate the graphitization of carbon materials.[16] Based on the Raman spectrum shown in Fig. S3, this ratio was calculated to be 2.8, which is much

larger than that for chemically reduced graphene oxides.[7,9] This result indicates that the GNS obtained by our method had a good graphitic structure. 2D and G bands indicate the key features of GNS. The 2D band peak at 2702 cm^{-1} is ascribed to the highest optical branch phonons near the K point at the Brillouin zone boundary and the G band peak at 1575 cm^{-1} is due to the two-fold degenerate E_{2g} mode at the Γ-point. The relative intensity ratio of I_{2D}/I_G can be used to estimate the number of layers of GNS. The integrity intensity ratios I_{2D}/I_G of >2, 1–2, and <1 correspond to single layered, double-layered and many-layered graphene, respectively.[17,18] The intensity ratio of I_{2D}/I_G in the present GNS is about 1.12, suggesting that the number of graphene layers is small.[19,20] In addition, thermal gravimetric analyzer (TGA, NETZSCH STA449F3) was employed to characterize the degree of graphitization for the sample of G2. From Fig. S4a (ESI†), we can see that this sample had an excellent resistance to oxidation as there was almost no weight loss at temperatures below 600°C. Such an observation is also indicative of that G2 had a well-developed graphitic structure. The mass percentage of Fe remained in the sample was estimated to be 3.5 wt.%, assuming that Fe_2O_3 was the only product after complete oxidation.

It is well known that it is very easy for $Fe(CO)_5$ to decompose at temperatures even as low as 100 °C. At the present experimental high temperatures, $Fe(CO)_5$ decomposed rapidly with the formation of iron nanoparticles, which possessed a very high catalytic activity for the decomposition of pyridine. Then, the carbon atoms produced were dissolved in iron, forming Fe-C intermetallic compounds. Since the amount of carbon source was limited, there was only a small amount of carbon atoms dissolved in iron particles. As the temperature decreased, a few graphitic layers formed on part of the surface of the iron particles. After the iron particles, which acted as substrates for C deposition, were removed, GNS were obtained.

Fig. S5a,b (ESI†) show the TEM images of sample G3. This sample consisted of hollow nanocages in addition to GNS. The shell thickness of nanocages (Fig. S5b) was ~8.13 nm. This observation indicates that controlling the ratio of carbon and iron at sufficiently low levels was a prerequisite condition for the preparation of GNS. Furthermore, increasing the reaction temperature from 900 to 1000 °C led to the formation of thicker graphite sheets with more than 10 graphitic layers as revealed by sample G4 (Fig. S5c,d, ESI†). Thus both the carbon and iron ratio and experimental temperature determined the sample morphology.

The advantage of using pyridine as the carbon source over other liquid carbon sources such as alcohol is that pyridine can be mixed with iron carbonyl at any ratios, and thus the ratio of carbon and Fe can be lowered for the preparation of GNS. The advantage of using iron carbonyl as the iron source is that iron particles act not only as a floating catalyst for the decomposition of pyridine but also as a floating substrate for the deposition of carbon. Consequently, GNS can be continuously produced and collected at the bottom of the reactor as long as the reaction solution is supplied into the reactor from the top. Under the experimental conditions for preparing G2 sample, 10 ml pyridine yielded about 1.2 g GNS power. For trial scaling up, the diameter of the reactor was increased from 3 to 10 cm, and the supplying rate of the reaction solution was increased from 5 to 50 ml min^{-1}, the production rate of GNS increased proportionally.

The present spray pyrolysis approach is different from previous ones. Although the reduction of graphene oxide can lead to mass production of GNS powder, this preparation method is complicated and time consuming as discontinuous processes of oxidation, exfoliation and reduction are involved.[7] CVD is an efficient method for synthesizing large-area graphene films.[13] But owing to the fact that the substrate is immovable, continuous preparation of graphene power is impracticable.

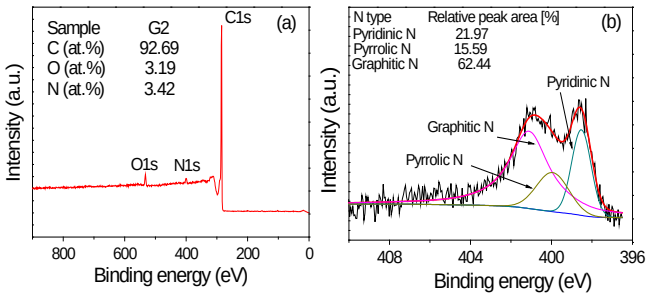

Fig. 2. XPS survey spectrum (a) and high resolution N 1s spectrum of G2 (b).

In this study, the use of pyridine (C_5H_5N) as the carbon resource was also designed to induce N doping into GNS, although the doping could also occur in the following process of heat treatment with NH_4Cl. X-ray photoelectron spectroscopy (XPS, Kratos Axis Ultra DLD) was carried out to evaluate the chemical composition on the surface of GNS. As shown in Fig. 2a, the survey spectrum of G2 confirms the presence of carbon (284.6 eV), nitrogen (400.1 eV), and oxygen (532.4 eV). The atomic percentage of nitrogen in sample G2 was 3.42%. The absence of any Fe peak in the XPS spectrum clearly indicates that no element of iron was detected on the surface of G2. To further investigate the bonding configurations of N atoms, high-resolution N 1s XPS spectrum of G2 was measured (Fig. 2b), which can be deconvoluted into three dominant peaks. The peak at 398.5 eV is assigned to pyridinic N, those at 399.9 and 401.1 eV to pyrrolic N and graphitic N, respectively, indicating the presence of N in different forms. [21]

N_2 adsorption/desorption isotherms (Macromeritics ASAP 2010N) were obtained to analyze the pore structure (Fig. S6, ESI†). The Brunauer–Emmett–Teller (BET) specific surface area of G2 was measured to be 195 $m^2 g^{-1}$, which is similar to the value for graphene sheets reported in literature.[22] As shown in Fig. S6a, the obvious hysteresis of desorption between the partial pressures P/P_0 of 0.5 and 1.0 suggests the existence of mesopores. The mesopore size distribution determined by the Barrett-Joyner-Halenda (BJH) method is shown in Fig. S6b. The average pore diameter is about 4 nm.

For possible catalytic applications in proton exchange membrane fuel cells (PEMFC), G2 was selected as a support material for Pt nanoparticles. TEM images clearly show that Pt particles dispersed on the surface of GNS uniformly with a narrow diameter distribution (Fig. 3a) and a diameter of about 3-4 nm (Fig. 3b). Fig. S7 (ESI†) shows the XRD pattern of Pt/GNS. The diffraction peak at 2θ = 26.16° is an overlapping of the wide peak for the diffraction of the (002) plane of few-layered graphene sheets at 23° and the sharp one for multi-layered graphene sheets with a good graphitic structure at 26°. The peaks at 2θ = 39.79°, 46.01° and 67.46° are related to Pt (111), Pt (200) and Pt (220), respectively. Based on the diffraction of (220) plane, the average particle size of Pt was calculated by Scherrer equation[23] to be 2.9 nm, which is consistent with the TEM measurement (Fig. 3b). The Pt loading on G2 support was estimated to be ~23.8 wt.% based on the TGA result shown in Fig. S4b (ESI†) after 3.5 wt.% residential Fe was excluded.

Electrochemically-accelerated durability testing (ADT) was employed to evaluate the long-term performance of catalysts in a three-electrode cell using a CHI618D instrument at a constant temperature. (The details of CV and ORR testing in 0.5M H_2SO_4 are described in the ESI†.) Pt/GNS and JM (Pt/C) catalysts exhibited the typical hydrogen desorption and adsorption peaks around 0-0.3V (Fig. S8a). At the beginning, the electrochemical surface area (ECSA) for Pt/GNS was slightly lower than that for Pt/C. However, Pt/GNS showed a higher durability.

Fig. 3c illustrates the ORR polarization curves of Pt/GNS and JM catalyst before and after ADT. It can be seen that both catalysts had a similar onset potential of about 900 mV before ADT cycling. In polarization curves, the half-wave potential $E_{1/2}$ (the potential corresponding to one-half of the diffusion current), was used to evaluate the ORR electrochemical activity of a catalyst. The $E_{1/2}$ for JM catalyst was about 732 mV, which was close to that for Pt/GNS (about 728 mV). The important observation was that Pt/GNS showed only a slight decline of 13 mV in $E_{1/2}$ after 1000 potential cycles. However, the JM catalyst exhibited a much larger potential degradation of 146 mV after 1000 potential cycles (Fig. 3d). After 3000 cycles, the $E_{1/2}$ for Pt/GNS (633 mV) is still much higher than that for JM catalyst (428 mV) (Fig. 3d).

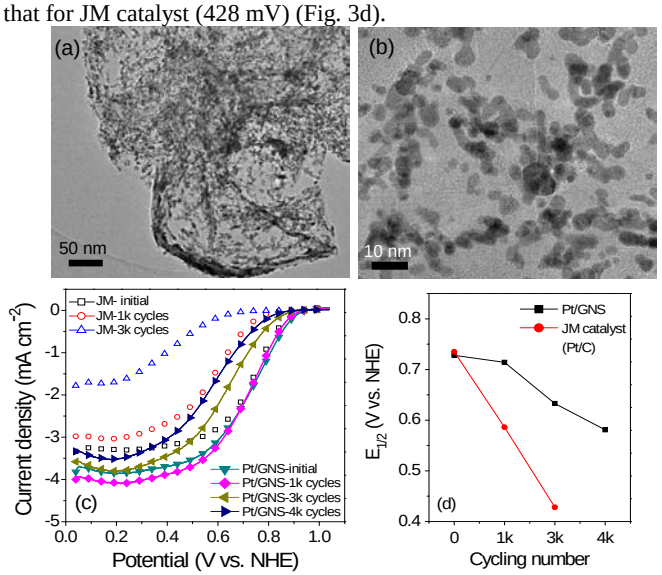

Fig. 3. TEM images of Pt/GNS (a, b), ORR polarization curves of Pt/GNS and JM catalysts in O_2-saturated 0.5 M H_2SO_4 (1600 rpm, scan rate: 5 mV s^{-1}) before and after CV cycling (c), and the variation of half-wave potential with cycling number.

The corrosion of the support material is a main reason for the degradation of catalysts, as the corrosion leads to the aggregation and detachment of Pt nanoparticles.[24] The stability of the support is related to its structure and composition. Enhancing graphitization is beneficial to durability improvement. As shown in Fig. 1d and Figs. S2 and S4, one of the characteristics of the present GNS is its well-developed graphitic structure and consequent high stability in the acidic electrolytic solution under the electrochemical condition. This may explain why the Pt/GNS catalyst exhibited little agglomeration of Pt particles after ADT testing (Fig. S9), compared to its initial state (Fig. 3b). In contrast, the support material for JM catalyst was amorphous carbon black (VXC-72) which could be easily corroded under the testing conditions.

On the other hand, the catalyst durability is also related to the interaction between Pt nanoparticles and supports. It has been reported that increasing the graphitization degree of carbon support leads to the enhanced π sites on carbon, and these sites act as anchoring centers for Pt nanoparticles.[25, 26] Thus, graphitization to a higher degree strengthens the interaction between Pt particles and the carbon support. At the same time, the electronic property of graphene could be modified owing to N doping and more active sites could be provided enhancing the interaction between the carbon structure and Pt crystals.[27] In this study, since the carbon source of pyridine contained N, in-situ N doping was achieved in the GNS with a good graphitic structure. This is another characteristic of the present GNS. The Pt-support interaction can thus be further strengthened as a result of N doping in the supports. Nitrogen in this case acts as ''tethers'' (chemical sites binding with Pt particles), which increases the catalytic activity not only by improving the dispersion of Pt particles but also by providing strong binding and thus resistance to nanoparticle agglomeration and coarsening.[28,29]

The Pt catalyst supported on the present highly graphitized GNS with N doping showed an excellent electrochemical durability. In comparison, the graphene prepared from reduction of graphene oxide often consisted of a large amount of defects resulting from the steps of graphite oxidation. These defects could not be reduced completely during the process of reduction, resulting in a low stability in acid media. Consequently, the Pt catalyst supported on such graphene demonstrated a low electrochemical durability.[30]

It has been reported that carbon nanomaterials with N doping show ORR catalytic activity because the electroneutrality of the sp^2-hybridized carbon atoms is broken by the dopants.[31] XPS result shows that there are N atoms on the surface of G2. Thus, for another potential application, G2 might be used as a metal-free catalyst for ORR in an alkaline medium. (The details of ORR testing in 0.1M KOH are described in ESI†)

The ORR polarization curves of G2 and JM catalyst in 0.1 M KOH solution before and after CV potential cycling are shown in Fig. 4a,b. At beginning, the half-wave potential for G2 was about 0.05 V, which is close to that for JM catalyst (about 0.1 V). The further important observation is that the $E_{1/2}$ for JM catalyst degenerated very quickly in the following potential cycling. However, the $E_{1/2}$ for G2 maintained unchanged (Fig. 4c), indicating a very good durability in the long term of potential cycling.

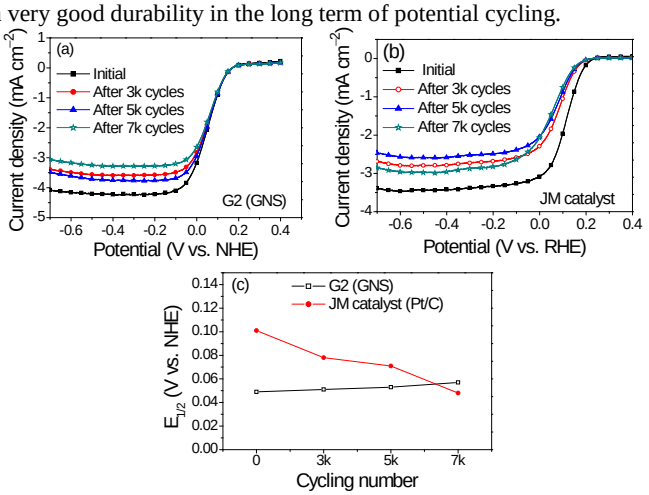

Fig. 4. ORR polarization curves of Pt free G2 (a) and JM catalyst (b) in O_2-saturated 0.1 M KOH (1600 rpm, scan rate: 5 mV s^{-1}), and the variation of half-wave potential with cycling number (c).

G2 possesses a similar property with the N-doped graphene from reduction of graphene oxide.[32] But, the electrochemical activity of the present N-doped GNS is close to Pt/C catalysts and better than other types of N doped carbon materials.[33-35] It may be further suggested that the N-doped GNS exhibits excellent electrocatalytic properties than disordered carbons due to its unique structural and electrochemical characteristics such as high specific surface area, conductivity, and uniform porosity.[36]

N-doping played a very important role for the electrocatalytic activity of G2 in ORR. XPS result in Fig. 2b suggests three types of N functionalities in G2, pyridinic N, pyrrolic N, and graphitic N. The high percentage of graphitic N could be responsible for the observed ORR activity as previously observed.[37,38] G2 metal-free catalyst also exhibited an excellent durability (Fig. 4c). The main reason for this may be the high degree of graphitization of the GNS, which could

provide a high corrosion resistance to the catalytic sites. This constitutes the further characteristic of the present N-doped GNS prepared by spray pyrolysis at high temperature.

In conclusion, a simple spray pyrolysis method was developed for the continuous preparation of GNS with high quality. The thickness of GNS could be controlled by adjusting the ratio of pyridine and iron carbonyl and experimental temperature. The GNS showed excellent performances when it was tested as a support material for Pt catalyst and as a metal-free catalyst for ORR. The main reason for this could be attributed to the well-developed graphitic structure and N doping in the present GNS.

Financial supports from National Natural Science Foundation of China (project #: 51271077, U1362104) and Shanghai Nanoscience and Nanotechnology Promotion Center (project #: 12nm0503300) are greatly acknowledged.

Notes and references

1 Y. Zhang, Y.-W. Tan, H. L. Stormer and P. Kim, *Nature*, 2005, **438**, 201.

2 A. A. Balandin, S. Ghosh, W. Bao, I. Calizo, D. Teweldebrhan, F. Miao and C. N. Lau, *Nano Lett.*, 2008, **8**, 902.

3 C. Lee, X. Wei, J. W. Kysar and J. Hone, *Science*, 2008, **321**, 385.

4 H. K. Chae, D. Y. Siberio-Pérez, J. Kim, Y. Go, M. Eddaoudi, A. J. Matager, M. O'Keeffe and O. M. Yaghi, *Nature*, 2004, **427**, 523.

5 K. S. Novoselov, A. K. Geim, S. V. Morozov, D. Jiang, Y. Zhang, S. V. Dubonos, I. V. Grigorieva and A. A. Firsov, *Science*, 2004, **306**, 666.

6 Y. Hernandez, V. Nicolosi, M. Lotya, F. M Blighe, Z. Sun, S. De, I. T. McGovern, B. Holland, M. Byrne, Y. K. Gun'Ko, J. J. Boland, P. Niraj, G. Duesberg, S. Krishnamurthy, R. Goodhue, J. Hutchison, V. Scardaci, A. C. Ferrari and J. N. Coleman, *Nat. Nanotech.*, 2008, **3**, 563.

7 W. Yuan, B. Li and L. Li, *Appl. Surf. Sci.*, 2011, **257**, 10183.

8 K. Erickson, R. Erni, Z. Lee, N. Alem, W. Gannett and A. Zettl, *Adv. Mater.*, 2010, **22**, 4467.

9 S. Stankovich, D. A. Dikin, R. D. Piner, K. A. Kohlhass, A. Kleinhammes, Y. Jia, Y. Wu, S. T. Nguyen and R. S. Ruoff, *Carbon*, 2007, **45**, 1558.

10 K. S. Kim, Y. Zhao, H. Jang, S. Y. Lee, J. M. Kim, K. S. Kim, J.- H. Ahn, P. Kim, J.- Y. Choi and B. H. Hong, *Nature*, 2009, **457**, 706.

11 P. W. Sutter, J.- I. Flege and E. A. Sutter, *Nat. Mater.*, 2008, **7**, 406.

12 J. Coraux, A. T. N'Diaye, C. Busse and T. Michely, *Nano Lett.*, 2008, **8**, 565.

13 P. Trinsoutrot, C. Rabot, H. Vergnes, A. Delamoreanu, A. Zenasni and B. Caussat, *Surf. Coat. Tech.*, 2013, **230**, 87.

14 H. Ueta, M. Saida, C. Nakai, Y. Yamada, M. Sasaki and S. Yamamoto, *Surf. Sci.*, 2004, **560**, 183.

15 W. Strupinski, K. Grodecki, A. Wysmolek, R. Stepniewski, T. Szkopek, P. E. Gaskell, A. Grüneis, D. Haberer, R. Bozek, J. Krupka and J. M. Baranowski, *Nano Lett.*, 2011, **11**, 1786.

16 M. Zhou, J. Tang, Q. Cheng, G. Xu, P. Cui and L.- C. Qin, *Chem. Phys. Lett.*, 2013, **572**, 61.

17 H. Medina, Y.-C. Lin, C. Jin, C.-C. Lu, C.-H. Yeh, K.-P. Huang, K. Suenaga, J. Robertson, and P.-W. Chiu, *Adv. Funct. Mater.*, 2012, **22**, 2123.

18 C. Shan, H. Tang , T. Wong, L. He and S.-T. Lee, *Adv. Mater.*, 2012, **24**, 2491.

19 X. Hu, Y. Zhang , H. Ago, H. Zhou, X. Li, L. Fan, B. Cai, X. Li, M. Zhong, K. Wang, D. Wu and H. Zhu, *Carbon*, 2013, **61**, 299.

20 A. C. Ferrari, J. C. Meyer, V. Scardaci, C. Casiraghi, M. Lazzeri, F. Mauri, S. Piscanec, D. Jiang, K. S. Novoselov, S.Roth and A. K. Geim, *Phys. Rev. Lett.*, 2006, **97**, 187401.

21 D. Geng, S. Yang, Y. Zhang, J. Yang, J. Liu, R. Li, T.-K. Sham, X. Sun, S. Ye and S. Knights, *Appl. Surf. Sci.*, 2011, **257**, 9193.

22 W. Ai, X. Cao, Z. Sun, J. Jiang, Z. Du, L. Xie, Y. Wang, X. Wang, H. Zhang, W. Huang and T. Yu, *J. Mater. Chem. A*, 2014, **2**, 12924.

23 Ch. V. Rao and B. Viswanathan, *J. Phys. Chem. C*, 2010, **144**, 8661.

24 W. Wang and Z. Ma, *Acta Phys.-Chim. Sin.*, 2012, **28**, 2879.

25 Y. Shao, G. Yin and Y. Gao, *J. Power Sources*, 2007, **171**, 558.

26 S. Wang, S. P. Jiang, T. J. White, J. Guo and X. Wang, *J. Phys. Chem. C*, 2009, **113**, 18935.

27 B. Xia, Y, Yan, X. Wang and X. Lou, *Mater. Horiz.*, 2014, **1**, 379.

28 S. Ye, A. K. Vijh and L. H. Dao, *J. Electrochem. Soc.*, 1997, **144**, 90.

29 T. Maiyalagan, B. Viswanathan and U. V. Varadarau, *Electrochem. Commun.*, 2005, **7**, 905.

30 D. He, K. Cheng, T. Peng, X. Sun, M. Pan and S. Mu, *J. Mater. Chem.*, 2012, **22**, 21298.

31 L. Qu, Y. Liu, J.-B. Baek and L. Dai, *ACS Nano*, 2010, **4**, 1321.

32 M. Vikkiska, I. Kruusenberga, U. Joostb, E. Shulgab, I. Kinkb, K. Tammeveskia, *Appl. Catal. B-Environ.*, 2014, **147**, 369.

33 A. Zahoor, M. Christy, Y. Hwang, Y. R. Lim, P. Kim, K. S. Nahm, *Appl. Catal. B- Environ.*, 2014, **147**, 633.

34 W. Ouyang, D. Zeng, X. Yu, F. Xie,W. Zhang, J. Chen, J. Yan, F. Xie, L. Wang, H. Meng and D. Yuan, *Int. J. Hydrogen Energy*. 2014, **39**, 15996.

35 Y. Zheng, Y. Jiao, L. Ge, M. Jaroniec, and S. Z. Qiao, *Angew. Chem. Int. Ed.* 2013, **52**, 3110.

36 L. Qu, Y. Liu, J. B. Baek, L. Dai, *ACS Nano*, 2010, **4**, 1321.

37 H. Kim, K. Lee, S. I. Woo, Y. Jung, *Phys. Chem. Chem. Phys.*, 2011, **13**, 17505.

38 L. Zhang, Z. Xia, *J. Phys. Chem. C*, 2011, **115**, 11170.

